# Magnetic and electronic properties of $CaMn_2Bi_2$: A possible hybridization gap semiconductor

Q. D. Gibson,[1] H. Wu,[2,3] T. Liang,[3] M. N. Ali,[1] N. P. Ong,[4] Q. Huang,[2] and R. J. Cava[1]
[1]*Princeton University, Department of Chemistry, Princeton, New Jersey 08544, USA*
[2]*NIST Center for Neutron Research, National Institute of Standards and Technology, Gaithersburg, Maryland 20899-6102, USA*
[3]*Department of Materials Science and Engineering, University of Maryland, College Park, Maryland 20742, USA*
[4]*Princeton University, Department of Physics, Princeton, New Jersey 08544, USA*
(Received 26 September 2014; published 27 February 2015)

We report the magnetic and electronic properties of $CaMn_2Bi_2$, which has a structure based on a triangular bilayer of Mn, rather than the $ThCr_2Si_2$ structure commonly encountered for 122 compounds in intermetallic systems. $CaMn_2Bi_2$ has an antiferromagnetic ground state, with a $T_N$ of 150 K, and for a 250 K temperature range above $T_N$ does not exhibit Curie-Weiss behavior, indicating the presence of strong magnetic correlations at high temperatures. Resistivity measurements show that $CaMn_2Bi_2$ exhibits semiconducting properties at low temperatures, with an energy gap of only 62 meV, indicating it to be a very narrow band gap semiconductor. The electronic structure of $CaMn_2Bi_2$, examined via *ab-initio* electronic structure calculations, indicates that Mn 3d orbital hybridization is essential for the formation of the band gap, suggesting that $CaMn_2Bi_2$ may be a hybridization-gap semiconductor.

DOI: 10.1103/PhysRevB.91.085128 PACS number(s): 71.20.−b, 75.50.Ee, 75.50.Pp

## I. INTRODUCTION

Layered transition metal compounds are of continuing interest in materials physics, exhibiting properties such as magnetism, superconductivity [1], charge density waves [2], and extremely large magnetoresistance [3]. The discovery of superconductivity in layered Fe-Se and Fe-As compounds [4–6] has revived interest in the layered Mn pnictides. With the recent discoveries of $BaMn_2Bi_2$ [7] and BaMnBiF [8] for example, Mn-Bi compounds have emerged as interesting analogs to the Fe based superconductors; they are expected to have lower band gaps and have easier accessible metallicity than other Mn pnictides due to the presence of the Bi layers. Here we report the electronic and magnetic properties of single crystals of hexagonal $CaMn_2Bi_2$, which exhibits unusual magnetism and a small band gap, with semiconducting transport properties. Further, through electronic structure calculations, we show that the hybridization of the Mn 3d orbital electronic states is important for imparting the semiconducting properties. From this we infer that $CaMn_2Bi_2$ is a candidate material for a hybridization gap semiconductor, in which localized states (such as d or f states) hybridize with a metallic band structure and form a band gap, such as in $Ce_3Bi_4Pt_3$ [9].

## II. EXPERIMENTAL

$CaMn_2Bi_2$ single crystals were grown using a Bi flux method [10]. Magnetic susceptibility, resistivity, and temperature dependent Hall and heat capacity measurements were taken on single crystal samples using a Quantum Design physical properties measurement system. Single crystals of mass 42 mg and 18 mg were used for the susceptibility and heat capacity measurements, respectively. A crystal cut into a bar of dimensions $1 \times 1 \times 2$ mm was used for transport measurements. Measurements of magnetization vs applied magnetic field were linear above the magnetic ordering transition to applied fields of $\mu_0 H = 1.0$ Tesla, and thus magnetic susceptibility is defined as $\chi = M/H$, where $M$ is the measured magnetization in that field. The field dependent Hall measurement was performed using a Keithley current sourcemeter and voltmeter. The orientation of the crystals for the single crystal transport and magnetic measurements was determined by single crystal x-ray diffraction. The natural facets were shown to be the 011 and 201 crystal faces. All transport data were taken within the (011) plane. The more intuitive [001] and [100] crystallographic directions could not be measured due to a lack of well defined facets corresponding to those directions.

Neutron powder diffraction (NPD) data were collected at the NIST Center for Neutron Research on the high resolution powder neutron diffractometer for various temperatures from 5 K to 295 K to elucidate the possible magnetic and crystal structure transitions. The temperature dependence of the peak intensity at the (100) magnetic reflection was monitored on warming to characterize the magnetic transition [11].

Electronic structure calculations were performed in the framework of density functional theory using the WIEN2K code [12] with a full-potential linearized augmented plane-wave and local orbitals basis together with the Perdew-Burke-Ernzerhof parametrization of the generalized gradient approximation [13]. The plane wave cutoff parameter $R_{MT}K_{max}$ was set to 7 and the Brilloun zone (BZ) was sampled by 2000 k points. LDA + $U$ calculations were also performed, with $U_{eff} = U - J$. Spin orbit coupling was included. The calculations were all performed with spin polarization, using the experimental antiferromagnetic configuration.

## III. RESULTS AND DISCUSSION

$CaMn_2Bi_2$ has a hexagonal structure [Fig. 1(a)] [14], related to the $ThCr_2Si_2$ structure found for the iron arsenide superconductors, as it is composed of layers of metal-pnictide tetrahedra separated by alkaline earth layers. The primary difference is in the geometry of the transition metal layers: In $CaMn_2Bi_2$, the Mn bilayer can be considered as a puckered Mn honeycomb, while in $ThCr_2Si_2$-type compounds such as $BaFe_2As_2$, the Fe plane is a simple square net.

 

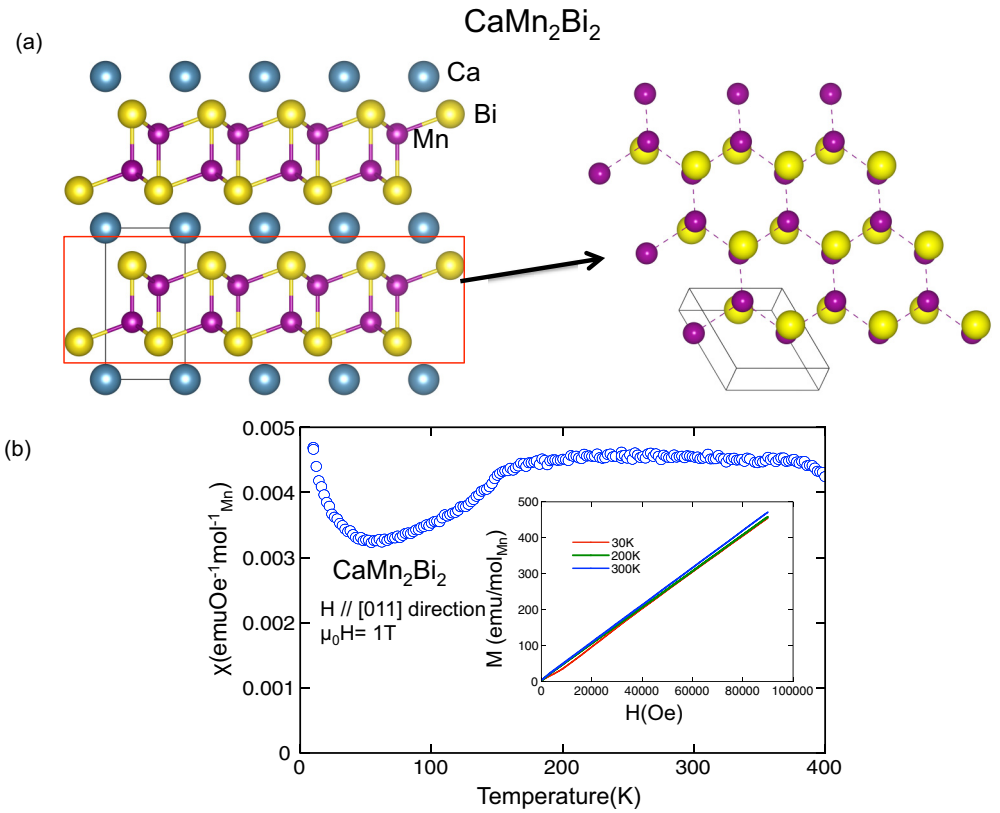


FIG. 1. (Color online) (a) The crystal structure of $CaMn_2Bi_2$ (left), and a top-down view of the Mn-Bi hexagonal sublattice (right). (b) Magnetic susceptibility versus temperature taken with $\mu_0 H = 1$ T. Inset: Magnetization versus applied field curve for three different temperatures.

The temperature dependent magnetic susceptibility for $CaMn_2Bi_2$ between 5 and 400 K is shown in Fig. 1(b). The susceptibility is almost temperature independent in the 400–150 K temperature range, with a broad weak peak that appears to be centered around 300 K. The susceptibility decreases quickly after a distinct change in slope on cooling below 150 K due to the presence of a magnetic phase transition, as confirmed by further measurements. Upon further cooling, the susceptibility levels off and then increases again at low temperatures. The low temperature increase is possibly due the presence of paramagnetic impurities (such as $Mn^{2+}$ ions occurring as defects); the low temperature behavior was sample dependent, while the higher temperature behavior was consistent across all samples. However the low temperature behavior being intrinsic cannot be completely ruled out. Figure 1(b) inset shows the magnetization versus applied field (MH) curves at 30, 200, and 300 K. The 300 and 200 K curves are linear for the whole field range up to 9 T. The 30 K curve, however, which is well below the magnetic ordering transition temperature, shows a slight field dependence, indicating that there may be some field induced spin canting or other mechanism disturbing the spontaneously ordered Mn moments in applied fields in the 2 Tesla or greater range.

Figure 2(a) shows the observed powder neutron diffraction pattern of $CaMn_2Bi_2$ at 5 K. The fitted curve includes both the refined crystal structure and magnetic structure models, indicating that both are well understood. The counts for the (100) diffraction peak, which is a magnetic diffraction peak, as a function of temperature, are shown in the inset of Fig. 3(a). This shows that the three-dimensional magnetic ordering begins at 154 K, consistent with the magnetic susceptibility measurements. The ordering transition follows a typical mean field behavior, with $I^2$ going as ($T_N$-T.) The 100 peak is shown to grow into the diffraction pattern in Fig. 2(b).

The magnetic ground state is antiferromagnetic (AFM), as shown in Fig. 2(c), with an ordered Mn moment at 5 K of $3.85\mu_B$, which is similar to that found in related systems [15–17]. The arrangement of Mn (or the magnetic structure) can be described using a Shubnikov magnetic space group of P-1' with opposite magnetic moments alternating between the nearest neighboring Mn atoms. The nearest neighbor Mn atoms in the bilayer have opposing spins; when considered as a puckered Mn honeycomb lattice, this alternating spin orientation ordering is a typical Neel state for honeycombs. Considered as Mn "bilayers," the coupling between neighboring bilayers is ferromagnetic, resulting in the magnetic unit cell being the same size as the nonmagnetic cell (though with a magnetic symmetry that allows the 100 reflection). This is the same type of antiferromagnetic ordering observed in similar systems such as $CaMn_2Sb_2$ and $BaMn_2Bi_2$ [15,16], i.e., nearest neighbor Mn atoms in-plane having opposite spins.

The phase transition at around 150 K was further studied by heat capacity measurements [Fig. 2(d)]. These measurements show a well-defined peak at around 150 K; no further phase transitions were observed in the 2–300 K temperature range. While the $T_N$ as derived from the neutron scattering appears

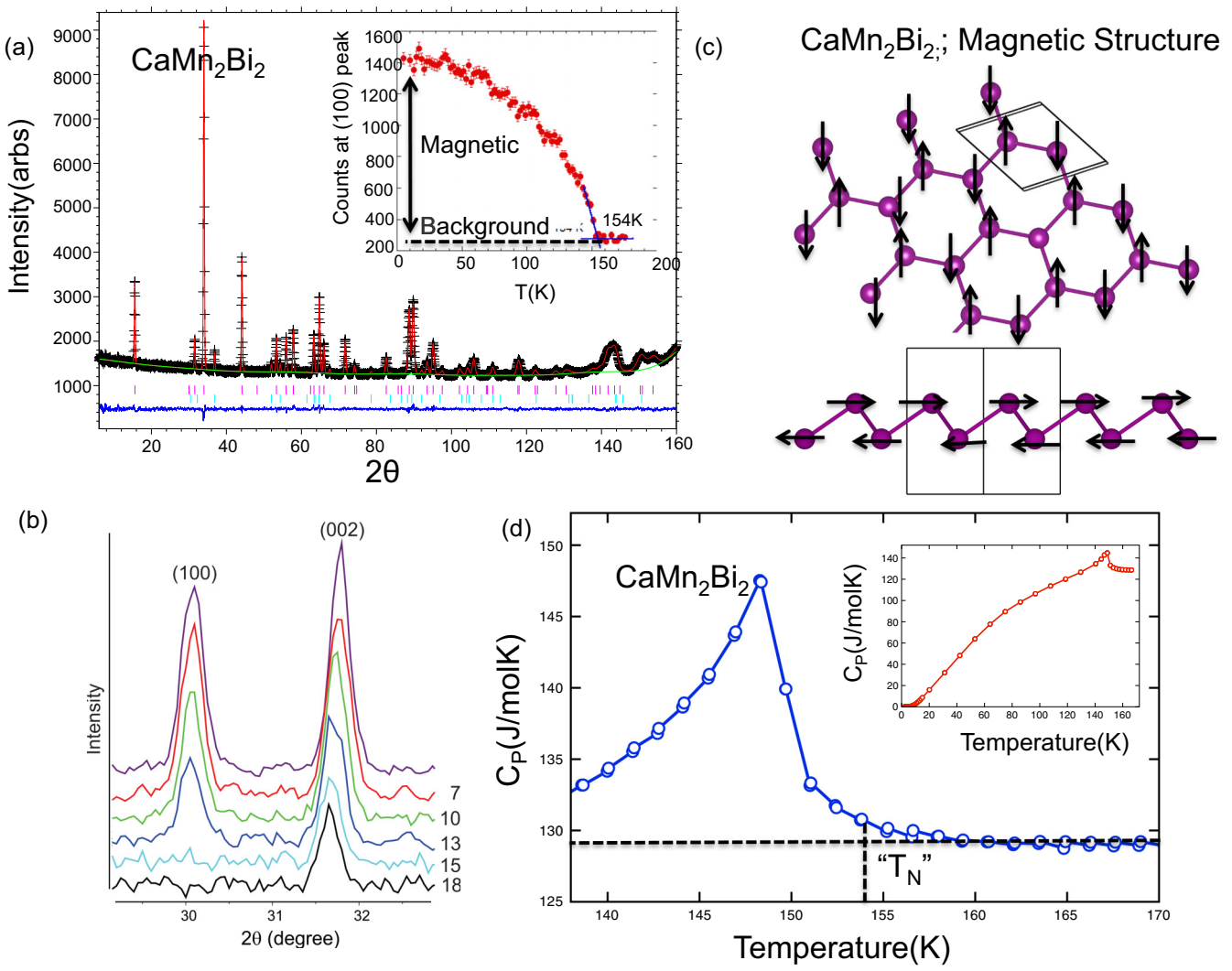


FIG. 2. (Color online) (a) Neutron diffraction pattern with the refined cell pattern overlaid. Inset: Counts of the (100) peak as a function of temperature, showing the transition temperature. (b) A plot of the intensity of the diffraction peaks at various temperatures, showing the growing in of the magnetic diffraction peak with temperature. (c) Two views of the magnetic structure of $CaMn_2Bi_2$ showing the spins alternating between nearest neighbor Mn atoms. Top: the Mn moment ordering from an overview of the puckered honeycomb sublattice. Bottom: a side view of the Mn sublattice. (d) Heat capacity versus temperature, showing the peak due to the AFM transition. The $T_N$ as derived from neutron scattering is labeled. Inset: Heat capacity over a wider temperature range.

to be higher than the temperature of the peak in the heat capacity, it is consistent with when the heat capacity appears to diverge from expected behavior; the $T_N$ is labeled on the figure. However, as there is no good nonmagnetic structural analog for $CaMn_2Bi_2$, the phonon contribution to the specific heat cannot be rigorously subtracted. The fact that the susceptibility in such a highly magnetic system is approximately temperature independent between 150 and 400 K, a range of about 250 K above the AFM ordering temperature, implies that local AFM correlations are very strong well above $T_N$; the magnetic moments are very likely short range ordered for a very wide range of temperature above $T_N$. In fact, the susceptibility bears some resemblance to a model of itinerant spin density wave (SDW) magnetism with a very small density of states [18]. Future work, including measuring other crystallographic directions, may reveal the nature of the magnetic behavior above $T_N$.

To further characterize the properties of $CaMn_2Bi_2$, resistivity and Hall effect measurements were performed. Figure 3(a) shows the resistivity behavior of a representative single crystal sample of $CaMn_2Bi_2$. $CaMn_2Bi_2$ crystals consistently exhibit "metallic" resistivity (resistivity that decreases with decreasing temperature) behavior between about 300 and 70 K, with a kink at 150 K due to the AFM transition. Below about 70 K, the resistivity shows activated behavior, and then levels off at a maximum value that is sample dependent. This leveling off of the resistivity could be due to either impurity or surface state conduction (see below).

The field and temperature dependent Hall resistivity curves for the samples in Fig. 3(a) are shown in Fig. 3(b). The curves show p-type behavior and are linear in field through a large temperature range. Below about 40 K, however, the Hall resistivity vs applied field curves become highly nonlinear, an indication of the presence of two carrier types.

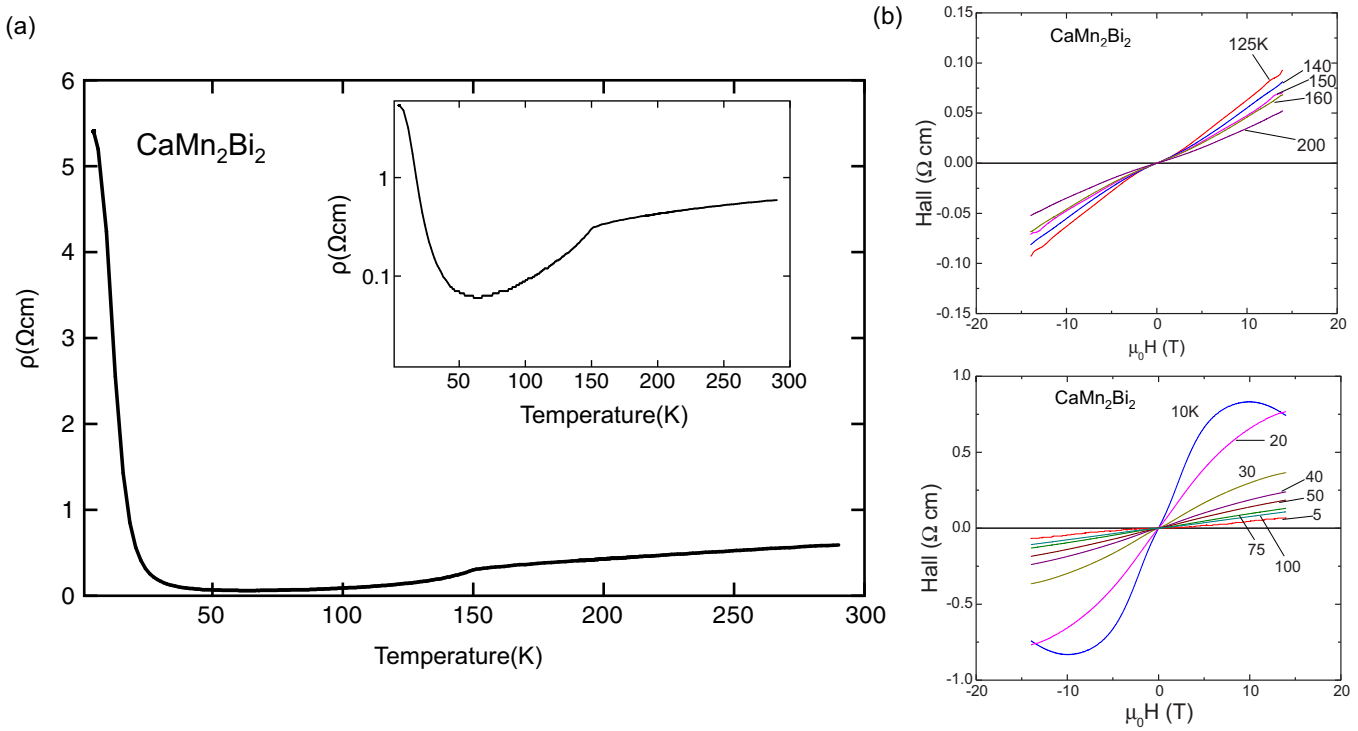


FIG. 3. (Color online) (a) Resistivity versus temperature for a representative single crystalline sample. A log scale is inset for clarity. (b) Hall resistivity versus field curves at various temperatures for a representative sample.

At low temperatures, consistent with the leveling off of the resistivity, the hall resistivity becomes linear again, and very small.

In order to understand the higher temperature "metallic" behavior of $CaMn_2Bi_2$, the temperature dependence of the resistivity and Hall resistivity were taken for another representative sample. The log resistivity vs 1/T plot for this sample is shown in Fig. 4 (upper panel). This figure shows the development of activated behavior, with $\frac{E_a}{k_b} = 11$ meV in the 20–50 K temperature range. In contrast with the resistivity, the Hall resistivity [Fig. 4(a), lower panel] shows activated behavior over the entire temperature range and does not change much through the AFM transition. This suggests that the AFM transition does not substantially affect the carrier concentration or Fermi surface, but instead primarily changes the carrier mobility likely due to decreased magnetic scattering. This indicates that the transport behavior is in the activated regime and that $CaMn_2Bi_2$ is semiconducting at all temperatures investigated, and that the "metallic"-like resistivity is due to a strongly temperature dependent mobility rather than actual metallic behavior.

The log $R_H$ vs 1/T plot is shown in the inset. Two regimes are observed, at high and low temperatures, with different activation energies. The low temperature activation energy is consistent with the one derived from the resistivity. The high temperature activation energy is larger, however, and likely related to the intrinsic band gap of the material. From the resistivity and hall data, the nominal hall mobility was calculated from 300 to 40 K [Fig. 4(b), lower panel inset], assuming one carrier type. (Because the Hall response becomes nonlinear below about 40 K, data is not shown below that temperature.) While there are likely both holes and electrons present even in the higher temperature regime, this data was used as an approximation, in order to understand the temperature dependence of the resistivity. The analysis shows that the nominal mobility increases upon cooling. A kink in the mobility is seen at the AFM transition. The mobility then increases dramatically before leveling off in the 40–50 K regime. $CaMn_2Bi_2$ therefore shows activated behavior throughout the entire temperature range; the "metallic" conductivity at high temperature is due to an increase in carrier mobility with temperature that is a stronger effect than the decrease in carrier concentration with temperature. A fit to the low temperature heat capacity [Fig. 4(c)] gives a Sommerfield coefficient $\gamma$ within error of 0, confirming the presence of very few charge carriers in the system at low temperatures. The low temperature resistivity and activation energy are both significantly smaller than the closest analogous compounds, $CaMn_2Sb_2$ and $BaMn_2Bi_2$ [19,20]. The resistivity is also consistent with the heat capacity; a large peak in the temperature derivative of the resistivity is seen near $T_N$ [Fig. 4(d)]; again $T_N$ is consistent with where the derivative begins to diverge from expected behavior. We note that the derivative of X(T)*T with respect to T shows a similar temperature dependence. However, due to very the small variation in X(T) in the 150–300 K region, this derivative is noisy and is not shown.

In order to understand the semiconducting behavior of $CaMn_2Bi_2$, electronic structure calculations were performed that included the experimentally determined AFM ordered state of the Mn. The electronic band structure is shown in Fig. 5(a). The calculations show that the conduction band near $E_F$ consists primarily of relatively nondispersive Mn 3d states, with one dispersive Bi(s)-Mn(s) hybrid band cutting through

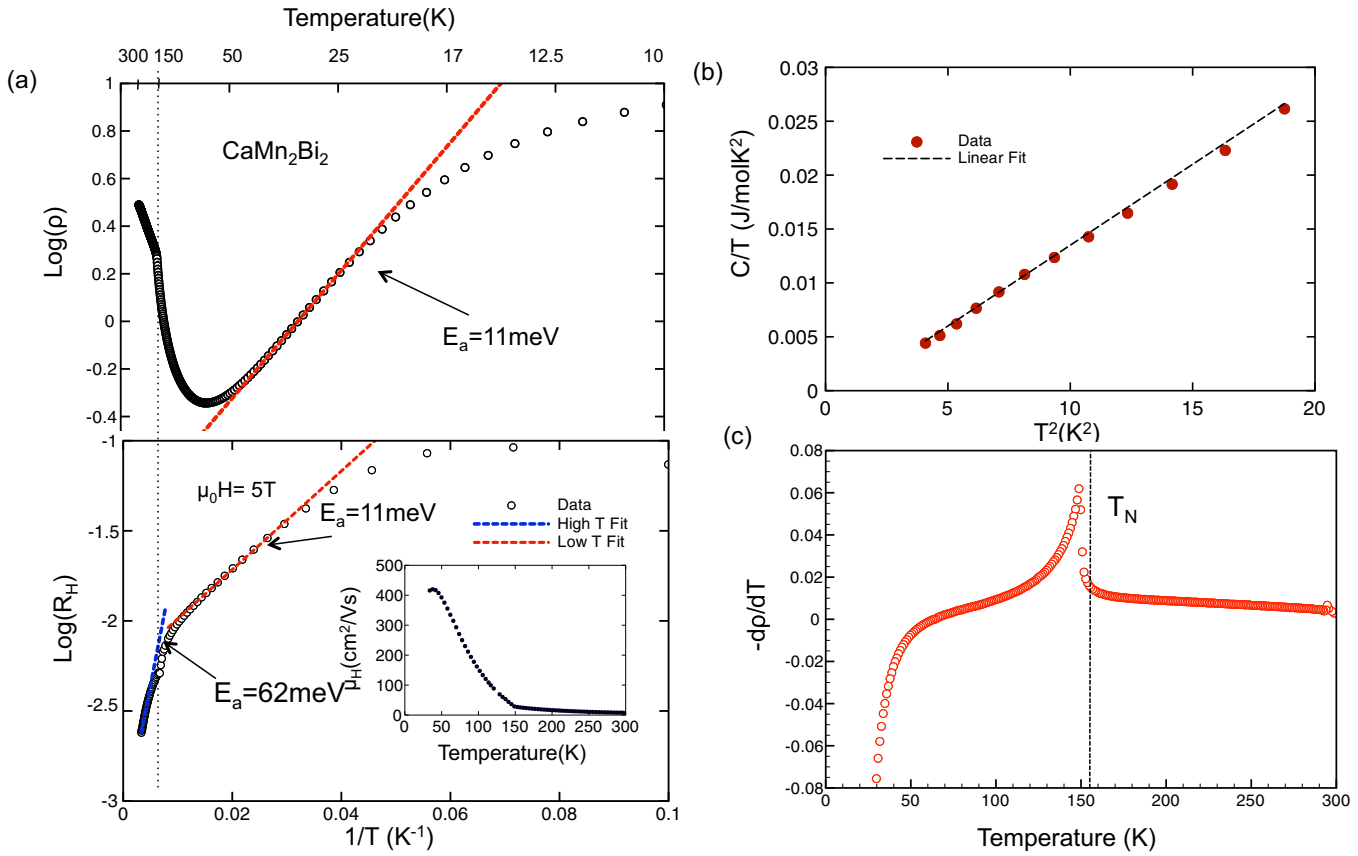


FIG. 4. (Color online) (a) A plot of the log of resistivity versus reciprocal temperature (top). The red dashed line is a linear fit, showing activated behavior. Bottom: a plot of the log of hall resistivity versus temperature, showing activated behavior with two regions. The blue line and red line are linear fits in the high temperature region and low temperature region, respectively. Inset: the nominal Hall mobility versus temperature. (b) A linear fit to C/T vs $T^2$. (c) A plot of $(-dp/dT)$ vs T showing a qualitative agreement with the heat capacity; the $T_N$ is labeled.

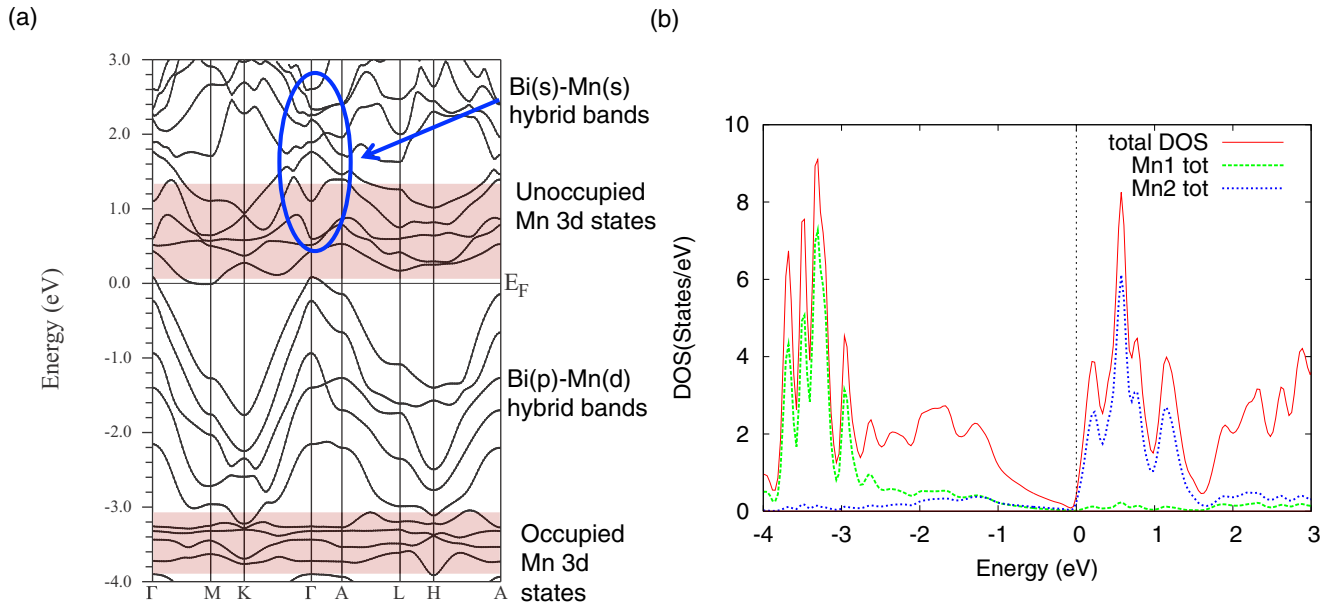


FIG. 5. (Color online) (a) Electronic band structure of AFM $CaMn_2Bi_2$. The AFM ordered Mn 3d states are highlighted in red, and states from the Bi-Mn s hybrid band are circled in blue. (b) The spin-up density of states (DOS) plot also showing the partial DOS of the Mn(1) and Mn(2) d states.

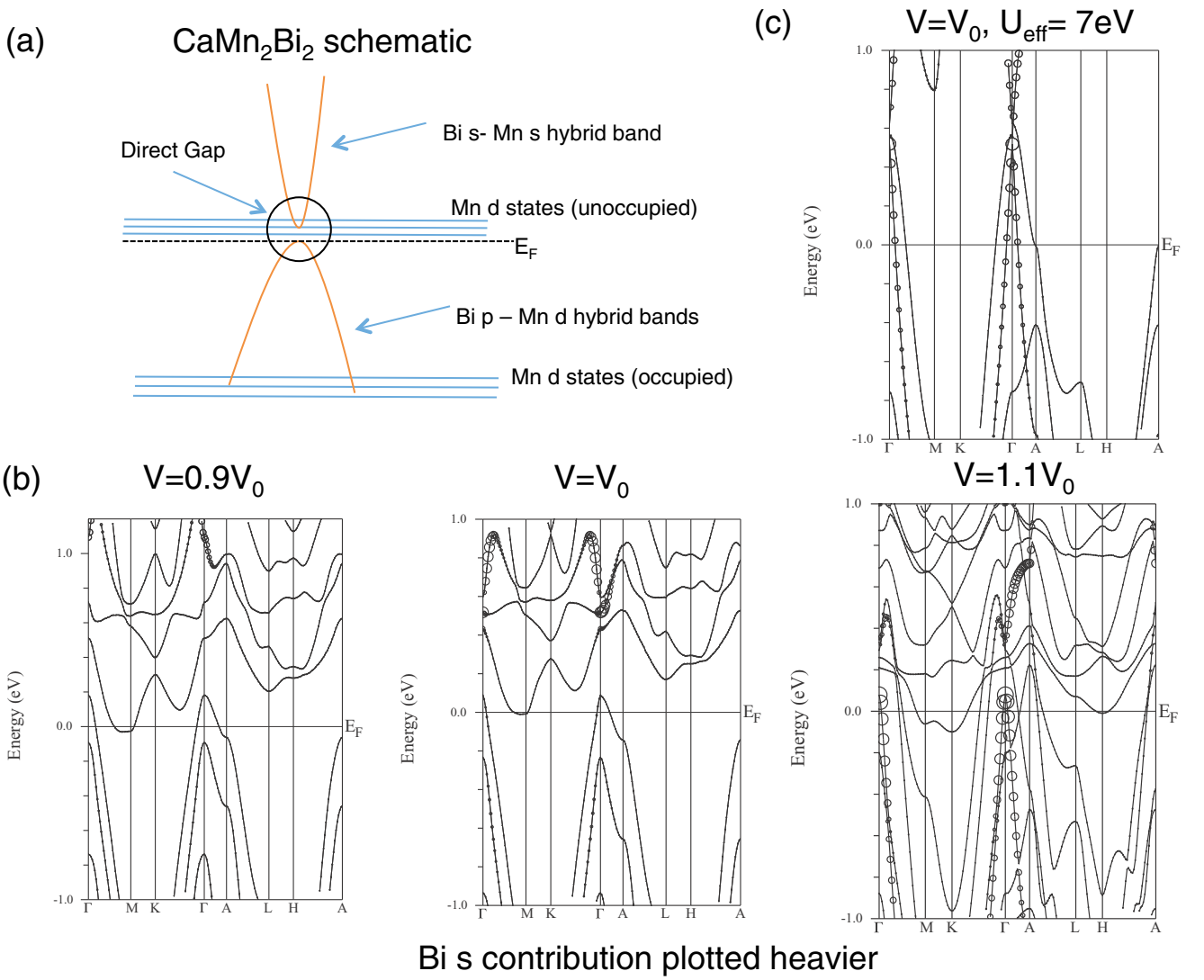


FIG. 6. (Color online) (a) Cartoon schematic of the electronic structure of $CaMn_2Bi_2$. (b) The band structure of $CaMn_2Bi_2$ at various volumes, with the Bi s states plotted heavier. Left to right: $0.9V_0$, $V_0$, and $1.1V_0$. (c) The band structure of the metallic state with $U_{\text{eff}} = 7$ eV.

them to the bottom of the conduction band. The Bi(s)-Mn(s) band refers to the fact that this band derives mainly from both Mn s and Bi s orbitals, indicating that the unoccupied Mn s states are strongly hybridized with the occupied Bi s orbitals. In contrast, the valence bands are composed of Mn (3d)-Bi(p) hybrid states. This calculation show a slight energy overlap between the valence band and conduction band states due to the usual DFT underestimation of the band gap, but the distinction between valance band and conduction band states is clear.

Figure 5(b) shows the calculated spin up density of states (DOS). [The spin down density of states is the same, with the Mn(1) and Mn(2) labels switched.] The DOS shows that essentially localized AFM ordered Mn d electron states—the E vs k behavior shows that bands are only weakly dispersive—are found just above $E_F$ and also at about 3 eV below $E_F$. There is also significant Mn d contribution in the valence band below $E_F$, from both spin up and spin down Mn atoms, at energies from 0 to $-3$ eV with respect to $E_F$. This second Mn contribution to the DOS in the valence band is representative of delocalized electrons, and the degeneracy of the Mn(1) and Mn(2) contributions means they are not impacted by the AFM ordering; the strongly hybridized Mn d states in the valence band are an important and large contribution. The calculated moment per Mn is $4.13\mu_B$ per Mn, which is very close to the observed ordered value. Thus both the experiment and the calculation imply that approximately one d electron per Mn atom is delocalized and hybridized with the Bi p states in the valence band, while the others are localized, giving rise to the observed large magnetic moment.

To illustrate what we propose is the overall electronic picture for $CaMn_2Bi_2$; a cartoon schematic of its calculated electronic structure is shown in Fig. 6(a). In order to understand the importance of the Mn d orbital hybridization on this electronic structure, additional calculations were performed with volume expanded and volume contracted lattices [Fig. 6(b)].

Upon lattice compression, the gap between the valence band and the Bi-Mn s hybrid band above $E_F$ becomes larger, while the indirect gap between the Mn d states in the conduction band and the valence band becomes very slightly smaller. Conversely, upon lattice expansion, the gap between the valence band and the Bi-Mn s derived conduction band decreases, even going through a metallic state at $V = 1.1V_0$. This is contrary to the normal behavior of materials, where compression of cell volumes increases the electronic hybridization and therefore decreases band gaps; here the opposite is found.

Similarly anomalous results were obtained by adding a coulomb repulsion term $U$ to the Mn 3d states in the calculation. Under normal circumstances the addition of the $U$ term is expected to push d electron states away from $E_F$ and prevent hybridization. Adding a $U$ term in this case does indeed have the effect of moving the 3d states away from $E_F$ but also, in contrast, it closes the gap between the top of the valence band and the Bi-Mn s band above $E_F$. By $U_{\text{eff}} = 7$ eV, a zero band gap state is calculated. That the calculated lattice expansion and coulomb repulsion effects are similar indicates that it is the hybridization of the Mn 3d orbitals that results in the very small band gap in $CaMn_2Bi_2$. The calculations imply that the hybridization of the Mn 3d states is actually required to make the compound semiconducting, as there is no gap when the hybridization is turned off, either by $U$ or by lattice expansion. This behavior is not expected for the usual semiconductor, but this exact mechanism of hybridization of localized states giving rise to a band gap is the proposed mechanism for all hybridization gap insulators, such as Ce based compounds like $Ce_3Bi_4PT_3$ [9] and for the Fe 3d based compound FeSi [21,22]. Given this, we infer that $CaMn_2Bi_2$ can be classified as an excellent candidate of a correlated hybridization gap semiconductor. The fact that strong Mn 3d-pnictide hybridization helps to open a band gap in this material may provide a generic reason why Mn pnictides tend to be insulators, while Fe pnictides tend to be metals or semimetals.

## IV. CONCLUSIONS

We report the magnetic and electronic properties of hexagonal layered $CaMn_2Bi_2$. This material was found to display antiferromagnetic ordering with a $T_N$ of 150 K along with strong antiferromagnetic suppression of the susceptibility, implying low dimensional antiferromagnetic ordering, for a temperature range of at least 250 K above $T_N$. Furthermore, $CaMn_2Bi_2$ is a narrow gap semiconductor, with a strong temperature dependence of the nominal hall mobility which leads to an apparent metallic resistivity. The high temperature transport gap is 62 meV while the low temperature gap is only around 12 meV. Band structure calculations indicate that Mn 3d orbital hybridization is key to opening the band gap, and that localized or quasilocalized Mn 3d orbitals dominate the conduction band just above $E_F$. We thus infer that $CaMn_2Bi_2$ is a correlated, antiferromagnetic, hybridization gap semiconductor. Further study into this or similar systems may elucidate the relationship between the correlated antiferromagnetic state of Mn and Fe pnictides and the superconductivity observed in Fe-As and Fe-Se compounds.

## ACKNOWLEDGMENTS

Q.D.G, M.N.A., and R.J.C. acknowledge support from SPAWAR Grant No. (NN6601-11-1-4110) and the AFOSR MURI Grant No. (FA9550-09-1-0953) N.P.O. and T.L. are supported by the Army Research Office (ARO W911NF-11-1-0379) and the National Science Foundation (Grant No. DMR 0819860). T.L. acknowledges scholarship support from the Japan Student Services Organization. We acknowledge helpful discussions with M. K. Fuccillo and N. Haldolarachchige.

[1] E. Morosan, H. Zandbergen, B. Dennis, J. Bos, Y. Onose, T. Klimczuk, A. Ramirez, N. Ong, and R. Cava, Nat. Phys. **2**, 544 (2006).

[2] G. Li, W. Hu, D. Qian, D. Hsieh, M. Hasan, E. Morosan, R. Cava, and N. Wang, Phys. Rev. Lett. **99**, 027404 (2007).

[3] M. N. Ali, J. Xiong, S. Flynn, Q. Gibson, L. Schoop, N. Haldolaarachchige, N. Ong, J. Tao, and R. Cava, Nature **514**, 205 (2014).

[4] X. Wang, Q. Liu, Y. Lv, W. Gao, L. Yang, R. Yu, F. Li, and C. Jin, Solid State Commun. **148**, 538 (2008).

[5] M. Rotter, M. Tegel, and D. Johrendt, Phys. Rev. Lett. **101**, 107006 (2008).

[6] F.-C. Hsu, J.-Y. Luo, K.-W. Yeh, T.-K. Chen, T.-W. Huang, P. M. Wu, Y.-C. Lee, Y.-L. Huang, Y.-Y. Chu, D.-C. Yan *et al.*, Proc. Natl. Acad. Sci. **105**, 14262 (2008).

[7] B. Saparov and A. S. Sefat, J. Solid State Chem. **204**, 32 (2013).

[8] B. Saparov, D. J. Singh, V. O. Garlea, and A. S. Sefat, Sci. Rep. **3**, 2154 (2013).

[9] M. F. Hundley, P. C. Canfield, J. D. Thompson, Z. Fisk, and J. M. Lawrence, Phys. Rev. B **42**, 6842 (1990).

[10] Crystals were grown from elemental starting materials in the ratio $CaMn_2Bi_{10}$. The elements were sealed in an evacuated quartz ampoule and heated to 1000 °C at 3 °C/min. The ampoule was held at 1000 °C for two days and then cooled to 400 °C at 0.1 °C/min and was centrifuged while hot to decant the excess Bi.

[11] Neutron diffraction measurements performed on diffractometer BT1, with monochromatic neutrons of wavelength 2.0775 Å produced by a Ge(311) monochromator. Soller collimations before and after the monochromator and after the sample were 60, 20, and 7 minutes full width at half maximum (FWHM), respectively. The diffraction measurements were taken on ground single crystals. Data were collected in the $2\theta$ range of 3 deg to 168 deg with a step size of 0.05 deg. Refinements of the nuclear and magnetic structures were carried out using the neutron powder diffraction data and the program GSAS [A. C. Larson and R. B. Von Dreele, Los Alamos National Laboratory Report No. LAUR086-748 (1990)]. The neutron scattering amplitudes employed were 0.490, −0.373, and 0.853 $cm^{-12}$ for Ca, Mn, and Bi, respectively.

[12] P. Blaha, K. Schwarz, P. Sorantin, and S. Trickey, Comput. Phys. Commun. **59**, 399 (1990).

[13] J. Perdew, K. Burke, and M. Ernzerhof, Phys. Rev. Lett. **77**, 3865 (1996).

[14] G. Cordier and H. Schäfer, Z. Naturforsch. B **31**, 1459 (1976).
[15] W. Ratcliff II, A. L. Sharma, A. Gomes, J. Gonzalez, Q. Huang, and J. Singleton, J. Magn. Magn. Mater. **321**, 2612 (2009).
[16] S. Calder, B. Saparov, H. Cao, J. Niedziela, M. Lumsden, A. Sefat, and A. Christianson, Phys. Rev. B **89**, 064417 (2014).
[17] A. Beleanu, J. Kiss, G. Kreiner, C. Köhler, L. Müchler, W. Schnelle, U. Burkhardt, S. Chadov, S. Medvediev, D. Ebke *et al.*, Phys. Rev. B **88**, 184429 (2013).
[18] M. Korshunov, I. Eremin, D. Efremov, D. Maslov, and A. Chubukov, Phys. Rev. Lett. **102**, 236403 (2009).
[19] K. Wang and C. Petrovic, Appl. Phys. Lett. **103**, 192104 (2013).
[20] J. W. Simonson, G. J. Smith, K. Post, M. Pezzoli, J. J. Kistner-Morris, D. E. McNally, J. E. Hassinger, C. S. Nelson, G. Kotliar, D. N. Basov, and M. C. Aronson, Phys. Rev. B **86**, 184430 (2012).
[21] Z. Schlesinger, Z. Fisk, H.-T. Zhang, M. Maple, J. DiTusa, and G. Aeppli, Phys. Rev. Lett. **71**, 1748 (1993).
[22] C. Fu, M. P. C. M. Krijn, and S. Doniach, Phys. Rev. B **49**, 2219(R) (1994).